Journal of Magnetic Resonance 281 (2017) 7–16

Contents lists available at ScienceDirect

Journal of Magnetic Resonance

journal homepage: www.elsevier.com/locate/jmr

Thin high-order shims for small dipole NMR magnets

Andrew McDowell [a,*], Mark Conradi [b,1]

[a] NuevoMR, LLC, 617 Amherst NE, Albuquerque, NM 87106, USA
[b] Washington University, Dept. of Physics, 1105, St. Louis, MO 63130, USA

ARTICLE INFO

Article history:
Received 17 January 2017
Revised 18 April 2017
Accepted 22 April 2017
Available online 24 April 2017

Keywords:
High-order shims
Miniaturized NMR
Matrix shims
Field homogeneity

ABSTRACT

An NMR shim coil design method that addresses the severe spatial constraints of miniaturized dipole magnets is introduced. The fundamental design element, a collection of straight wires, is shown to be sufficient for producing a complete set of shim fields of high mathematical order. In accord with these theoretical considerations, a shim set is constructed using four wires in each of four directions to create all first through fourth order fields, except one. This shim set, with its supporting structure, occupies only 2 mm of the available 5 mm gap in a small 1.6 T magnet. However, the fields produced by the individual wires are found to differ significantly from theoretical expectations. To produce the desired harmonic shim fields, the magnetic field of each of the 32 wires is mapped in three dimensions, and linear combinations of these maps are formed. The resulting shim fields are found to be very pure. The shims are used in a prototype high-resolution NMR magnet in which the 1.0 mm sample size is only possible due to the thinness of the shim set. The resulting spectra demonstrate shimming to high resolution (<25 ppb FWHM) without undue heating effects.

© 2017 Elsevier Inc. All rights reserved.

1. Introduction

Although the subject dates to the early days of experimental NMR, the topic of active shim design continues to generate new ideas and publications. The early analytical approaches [1,2] focused on developing orthogonalized shim sets using analytical techniques applied at the center of the sample space. Seeking a larger operating volume, Turner [3] introduced the target field method which considered fields at the outer surface of the sample. Coils designed with this approach could be quite long, so size constraints were added, although some found that the resulting designs could be difficult to construct due to localized regions of high current density [4,5]. The effect can be pronounced for the bi-planar geometry used in dipole magnets, as summarized by Liu [6]. Researchers have attacked this and other practical concerns through design methods based on simulated annealing [7], genetic algorithms [8,9], boundary element methods [10], linear programming [11], new hybrid analytical methods [6], and others, and work has continued in recent years (see, for example, Refs. [12–14]). The inclusion of practical constraints poses real challenges to the seemingly solved mathematical exercise of shim coil design.

One such practical constraint that has not been addressed directly is the need for space efficiency. This need is prominent for those working with miniaturized magnet systems [15,16] for NMR. Conventionally constructed active shim coils, no matter how designed, can readily require a number of millimeters of thickness to achieve corrections to high mathematical order. If one is starting with a dipole magnet sporting a 5 mm gap [15], for example, the shim coils may fill all of the working volume in the device. To fully realize the advantages of using very small magnets for high-resolution NMR, a shim design that can be constructed to use only a small amount of the gap space is needed.

We have found it useful to return to the early work of Anderson [2] on shim designs for the large NMR electromagnets at Varian. As we discuss in detail below, his basic design element is the infinite straight wire. His goal is to find arrangements of such wires that produce the desired orthogonalized shim set. By considering the production of fields (at the center of the magnet) of distinct mathematical order, Anderson arrives at a set of readily constructed shim patterns. There is nothing in Anderson's design methodology that limits it to low order fields, only the mathematical tractability of the analytical problems to be solved.

Today, we have nearly limitless computational power and facile field measurement methods that allow us to refine and extend Anderson's ideas in useful new ways [17]. We employ only straight wires that fully traverse the space-limited gap region. Each layer of the shim structure contains only parallel wires, so no wire

* Corresponding author.
E-mail address: mcdowell@nuevomr.com (A. McDowell).
[1] Present address: ABQMR, Inc., 2301 Yale Blvd. SE, Albuquerque, NM 87106, USA.

http://dx.doi.org/10.1016/j.jmr.2017.04.013
1090-7807/© 2017 Elsevier Inc. All rights reserved.

crossings are needed, and the currents are returned to their source outside of the space-limited gap region. This avoids the build-up of thickness that would fill our limited gap. Moving beyond Anderson's results, we allow for more wires and for each one to carry an independently set current. Hence, we require many more channels of current control and a more sophisticated method for adjusting these currents. Our approach trades a substantial increase in the complexity of the electronics and software *outside* the magnet in order to have a dramatic simplification of the physical shim structure *inside* the magnet.

In this article, we design, construct, and characterize such a shim set. The theoretical underpinnings of the work are discussed first. However, we show that the actual fields produced by wires in our dipole magnet differ substantially from theoretical expectations. To realize the harmonic shim fields that the theory indicates are possible, we make a 3D map of the field produced by each individual wire, and find the linear combinations of these maps that produce the desired shim fields. The mathematical purity of the resulting fields is measured and discussed. We apply our design in a prototype miniaturized NMR magnet and show that high-resolution can be achieved without undue heating.

2. Fundamental considerations

The fundamental fact underlying this work is that the z-component of a magnetic field satisfies Laplace's Equation in a source-free region:

$$\nabla^2 B_z = 0 \tag{1}$$

(As is usual in discussing shims for NMR, we can ignore the B_x and B_y components since the shim fields are perturbing a very much larger field in the z-direction.) Eq. (1) greatly limits the number of allowed functional forms for B_z expressed in terms of the spatial coordinates x, y, and z. Anderson captures this feature of the problem in his tabulation of the possible derivatives of the magnetic field of a long straight wire carrying current parallel to the x-axis. His geometry, which we will also utilize, is shown in Fig. 1. In panel (a), the region between the poles of a dipole magnet is sketched in perspective view, with one wire on the plane at $z = +Z_0$, oriented parallel to the x-axis and placed offset from the middle of the plane at location $y = +Y_0$. This wire is described as having a value of $\eta \equiv Y_0/Z_0$. In Anderson's designs multiple such wires, at different values of η, placed on both the $+Z_0$ and $-Z_0$ planes, act together to form the individual first and second order shim fields. Generally, the wires in his designs all carry the same current, so that each individual shim may be formed from one continuous wire.

Anderson expressed the spatial dependence of the field produced by the wire at (Y_0, Z_0) as:

$$B_z(Y,Z) = \frac{\mu_0 I_x}{2\pi} \frac{(Y - Y_0)}{(Y - Y_0)^2 + (Z - Z_0)^2}, \tag{2}$$

and he expressed the derivatives of this field, evaluated at $Y = 0$, $Z = 0$ (the center of the magnet gap), as functions of $\eta = Y_0/Z_0$. The goal of his design method is to produce these field derivatives one at a time, using a small set of wire locations, η. In this he is aided significantly by symmetry considerations. The sets of wires always include the four symmetry-related positions shown schematically in Fig. 1(b). The wire labeled 1 is at the same position as the one shown in panel (a), while the wires 2, 3, and 4 are the locations found via reflections in the $Y = 0$ and $Z = 0$ planes. If each wire carries the same current into the page, they each create the same magnitude of B_z at the origin, but in different directions, as shown by the arrows in panel (b). The total B_z is zero at the origin, due to the pairwise cancellation of the fields from wires 1 & 4 and 2 & 3. At a point

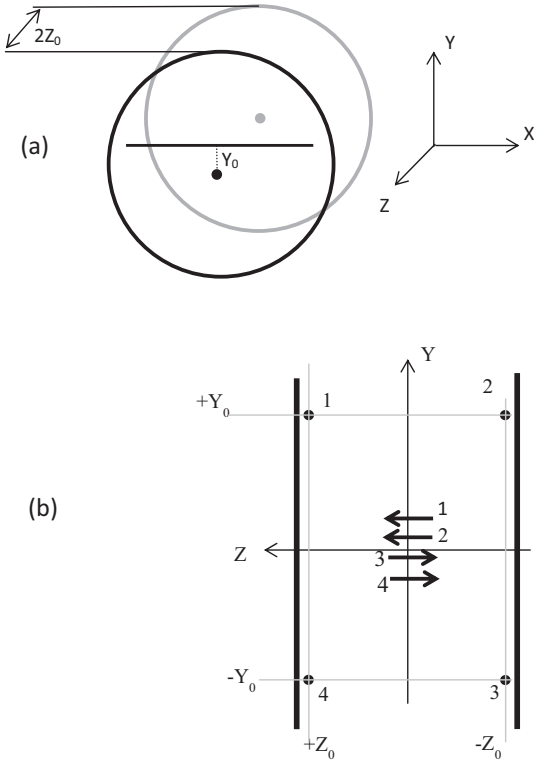

Fig. 1. The magnet gap geometry. The shim wires will be placed in one of two planes, at $\pm Z_0$, near each of the two pole faces shown in (a). An example wire is shown in (a) on the $+Z_0$ plane. The gap as seen from the end of the X axis is shown in (b). Here, four wires are shown: the wire in panel (a) and the symmetry-related wires. The arrows depict magnetic fields at the origin and are discussed in the text. The solid vertical bars just outside of the wire locations represent the magnet poles.

on the y axis slightly above the origin, the pairwise cancellation no longer holds and the total field will be non-zero. Slightly below the origin, the field is also non-zero, but of opposite sign. Small displacements along the Z axis, however, have no effect to first order, since the fields from wires 1 and 4 will still cancel, as will the fields from wires 2 and 3. Hence, for this situation where the wire locations and currents are symmetric both with respect to Y and to Z, the wires can produce only odd derivatives of Y and even derivatives of Z. A more complete consideration of symmetry shows that current distributions symmetric in Y produce odd derivatives of Y, while those antisymmetric in Y produce even derivatives. For Z, the result is reversed: symmetric current distributions produce even Z derivatives, while anti-symmetric designs produce odd derivatives.

Anderson uses these symmetry considerations, together with his expressions for the strength of the derivative terms, to find appropriate η values to make each individual derivative function while eliminating the next allowed function. He then constructs his shim set by winding one wire along the calculated paths, and in the correct orientation, for each mathematical term he includes in his shim set.

For our work, we prefer to work directly in expressions for B_z, rather than its derivatives. Eq. (2) may be Taylor-expanded according to

$$B_Z(Y,Z) = \frac{\mu_0 I_x}{2\pi Z_0} \sum_{n_y=0}^{\infty} \sum_{n_z=0}^{\infty} \frac{(Y)^{n_y} (Z)^{n_z}}{n_y! n_z!} \left[\frac{\partial^{n_y+n_z}}{\partial^{n_y} Y \partial^{n_z} Z} B_z(Y,Z) \right]_{Y=0,Z=0} \tag{3}$$

It is useful to group the terms for each order $N = n_y + n_z$ and separately sum the terms whose n_y are even and those for which n_y is odd. These summed terms are tabulated in Table 1, separated into the part that depends on the spatial coordinates (Y,Z) in the magnet

Table 1
Fields due to wire parallel to x axis.

Order (N)	Spatial Function	Eta Function	Current Symmetry	
			Z	Y
1	$T_{1E} = Y$	$C_{1E} = \frac{1-\eta^2}{(1+\eta^2)^2}$	+	+
	$T_{1O} = -2Z$	$C_{1O} = \frac{\eta}{(1+\eta^2)^2}$	−	−
2	$T_{2E} = 2YZ$	$C_{2E} = \frac{1-3\eta^2}{(1+\eta^2)^3}$	−	+
	$T_{2O} = Y^2 - Z^2$	$C_{2O} = \frac{\eta(3-\eta^2)}{(1+\eta^2)^3}$	+	−
3	$T_{3E} = 3YZ^2 - Y^3$	$C_{3E} = \frac{\eta^4-6\eta^2+1}{(1+\eta^2)^4}$	+	+
	$T_{3O} = 12Y^2Z - 4Z^3$	$C_{3O} = \frac{\eta(1-\eta^2)}{(1+\eta^2)^4}$	−	−
4	$T_{4E} = 4YZ^3 - 4Y^3Z$	$C_{4E} = \frac{5\eta^4-10\eta^2+1}{(1+\eta^2)^5}$	−	+
	$T_{4O} = 6Y^2Z^2 - Y^4 - Z^4$	$C_{4O} = \frac{\eta(\eta^4-10\eta^2+5)}{(1+\eta^2)^5}$	+	−

For order N, one of the fields created at the origin is $B_{NE} = \frac{\mu_0 I}{2\pi}\frac{1}{Z_0^N} T_{NE} C_{NE}$

gap (the T-functions) and an amplitude term dependent on the location of the wire, η (the C-functions). The η functions are those calculated by Anderson. For each mathematical order, N, there are two spatial functions. These are the only two unique functions of that order that satisfy Laplace's Equation, and hence they form a basis set for the expansion of any function that satisfies that equation. We will refer to this as the "straight wire basis set." The low order functions are recognizable as elements in a typical NMR shim set. The higher order functions are useful for constructing higher order shims by combination. Table 1 also indicates the required current value symmetry (+) or asymmetry (−) with respect to Z and Y when multiple symmetrically located wires are used to produce these functions.

The functions C_{NE} and C_{NO}, which express the role of wire location (η), are plotted in Fig. 2. For a current distribution of distinct y-symmetry, the sum of either the E or O functions for all four wires must be identically zero and only one of Fig. 2(a) or Fig. 2(b) must be considered. Furthermore, for an arrangement of distinct z-symmetry, only half of the remaining functions must be considered. For example, for a current distribution symmetric (+) in both y and z, Table 1 shows that the only possible non-zero terms (considering only terms of order $N \leq 4$) are C_{1E} and C_{3E}, with corresponding spatial functions $T_{1E} = Y$ and $T_{3E} = 3YZ^2 - Y^3$. For a single choice of η for which C_{1E} and C_{3E} are non-zero, the four wires carrying a common amplitude of current will produce both T_{1E} and T_{3E} in a fixed ratio. By including two appropriate values for η, the eight wires carrying a common current can make one of these fields without producing the other.

We choose to allow all wires to carry independent currents. The motivation for doing so is the recognition that symmetry considerations are important when one wants to produce only a single one of the basis set functions, but that any real-world magnetic field will require some linear combination of these functions in order to correct its field inhomogeneities. Allowing for independent currents allows us to produce the required linear combination from a single set of straight wires; we do not require a separate wire pattern for each of the basis set functions. In principle, we also allow for a multitude of wire locations. By letting each of many straight, parallel wires carry an independent current we can produce any one of the functions in Table 1, and hence any linear combination of these functions, with a thin, single-layer structure.

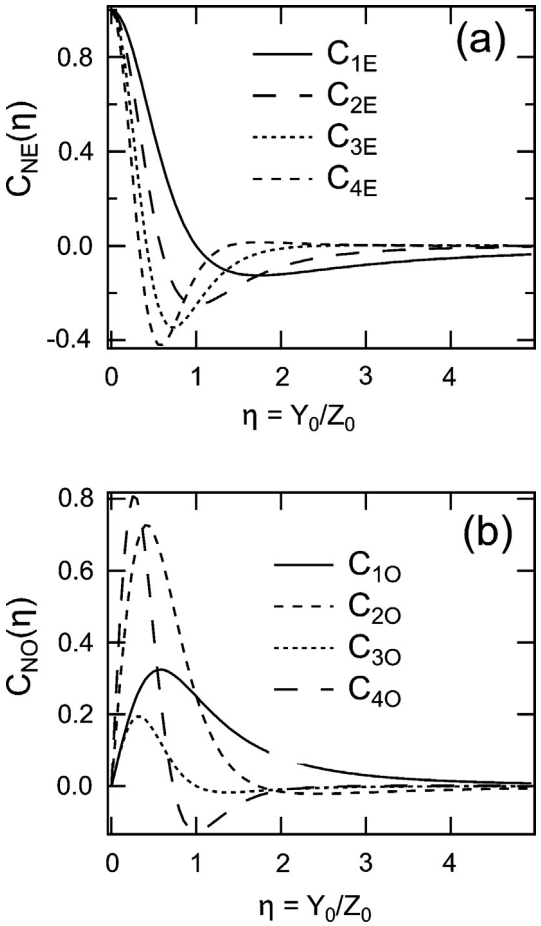

Fig. 2. The η functions of Table 1. These functions describe the strength and sign of the contributions to B_z at the origin, for a wire at a location specified by $\eta = Y_0/Z_0$.

3. Producing harmonic fields

Sets of shim coils in NMR are usually described in terms of real-valued spherical harmonic fields. This basis is both familiar and useful. One readily recognizes whether a shim set is complete or not if it is labeled using this basis, this basis has useful mathematical properties (notably orthogonality) that makes the shim set easier to use, and there is a great deal of experience and institutional knowledge aimed at the efficient adjustment of shim sets described in terms of this basis. Hence, we now consider how our straight wire basis can be transformed into the more familiar spherical harmonic functions.

The real-valued spherical harmonics may be expressed [18]:

$$(n,m) \equiv (-1)^m \sqrt{\left(\frac{2n+1}{2\pi}\right)\frac{(n-m)!}{(n+m)!}} P_n^m(\cos(\theta)) \begin{cases} \cos(m\varphi) & m \geqslant 0 \\ \sin(m\varphi) & m < 0 \end{cases} \quad (4)$$

These are the atomic orbitals expressed in the familiar angular variables. These functions are written in terms of Cartesian coordinates in Table 2 for orders 1 through 4. Those with experience in shimming NMR spectrometers will recognize many of these functions as labels of particular shims in a typical shim set. Table 2 also contains columns indicating the symmetries in the current values with respect to both z and the transverse variables (x & y) when multiple symmetrically located wires are used to create these fields.

The spherical harmonics have distinct symmetries with respect to their x & *y* and their *z* dependencies, so they are mathematically similar to the straight wire basis functions. Comparing Tables 1 and 2, one sees that the straight wires in one direction already are making some spherical harmonics: (1,0), (1,−1) and (2,−1), otherwise known as the Z, Y, and YZ fields. It is also clear that wires in a single direction cannot form a complete set for shimming, since the (1,1), e.g. X, term is missing. This is easily corrected by adding wires in another direction, parallel to the *y* axis rather than *x*. These new wires make fields of the form X (1,1), XZ (2,1), $X^2 - Z^2$, $3XZ^2 - X^3$- and so on. We will refer to the new functions as T_{NE}^{90} and T_{NO}^{90}, while the original functions tabulated in Table 1 are given the superscript 0. The spherical harmonic functions (2,0) and (2,2) can be formed by symmetric and antisymmetric combinations of T_{2O}^{0} and T_{2O}^{90}. The only second order function that can't be made with wires in these two directions is (2,−2) = XY. Fig. 3 shows a photograph of an example shim paddle with wires in two perpendicular directions. This simple paddle, together with its compatriot placed on the other pole of the magnet, forms a shim set capable of making all first order fields and all but one second order field.

There is a basic counting argument at play here. Each wire orientation can contribute 2 independent functions at each mathematical order (a consequence of Laplace's Equation). There are five linearly independent second order fields, and the two wire directions considered so far can produce at most 4 independent N = 2 functions. To produce the missing second order field, wires in a new direction are needed. Mathematically, only one more orientation is needed, but it is more pleasing to add two: along the X = Y and X = −Y diagonals, which create the fields T_{NE}^{45}, T_{NO}^{45}, T_{NE}^{135}, and T_{NO}^{135}. The two new directions are just the same shim set rotated by 45 degrees. Since the (2,−2) field is just the (2,2) field rotated by 45 degrees, the new wires will be able to make (2,−2).

The shim set containing wires in four directions can make all the first and second order spherical harmonic fields and so this design forms a complete shim set for these two orders. The counting argument implies that the four orientations would also be able to contribute eight 3rd order fields, eight 4th order fields, and so on. This is correct. We have written out all the *T*-functions for each orientation of wires and found linear combinations of these that produce all the third order (3,*m*) fields and all but one of the fourth order (4,*m*) fields (not shown here). For example, the (3,*m*) functions in Table 2 require current distributions that are either (i) antisymmetric with respect to both z and x & y or (ii) symmetric with respect to both. Hence, the symmetry information in Table 1 indicate that case (i) functions are constructed from T_{3O}^{0} and its rotated versions, while case (ii) functions are built out of T_{3E}^{0} and its rotated versions. There are nine fourth order elements in the spherical harmonic basis, so the eight functions from the straight wires in four directions cannot span the full fourth-order mathematical space. The missing harmonic term is the (4,−4) field; if it is needed, another new wire direction can be added to the shim set.

Table 2
Real valued spherical harmonic terms.

(*n*,*m*)	Un-normalized Cartesian Function	Current Symmetry	
		Z	X & Y
(1,0)	Z	–	–
(1,1)	X	+	+
(1,−1)	Y	+	+
(2,0)	$2Z^2 - X^2 - Y^2$	+	–
(2,1)	XZ	–	+
(2,−1)	YZ	–	+
(2,2)	$X^2 - Y^2$	+	–
(2,−2)	XY	+	–
(3,0)	$Z(2Z^2 - 3X^2 - 3Y^2)$	–	–
(3,1)	$X(4Z^2 - X^2 - Y^2)$	+	+
(3,−1)	$Y(4Z^2 - X^2 - Y^2)$	+	+
(3,2)	$Z(X^2 - Y^2)$	–	–
(3,−2)	XYZ	–	–
(3,3)	$X(X^2 - 3Y^2)$	+	+
(3,−3)	$Y(Y^2 - 3X^2)$	+	+
(4,0)	$8Z^4 + 3(X^4 + Y^4) - 24Z^2(X^2 + Y^2) + 6X^2Y^2$	+	–
(4,1)	$XZ(4Z^2 - 3(X^2 + Y^2))$	–	+
(4,−1)	$YZ(4Z^2 - 3(X^2 + Y^2))$	–	+
(4,2)	$(X^2 - Y^2)(6Z^2 - (X^2 + Y^2)) = 6Z^2(X^2 - Y^2) - X^4 + Y^4$	+	–
(4,−2)	$XY(6Z^2 - (X^2 + Y^2))$	+	–
(4,3)	$XZ(X^2 - 3Y^2)$	–	+
(4,−3)	$YZ(Y^2 - 3X^2)$	–	+
(4,4)	$X^2(X^2 - 3Y^2) - Y^2(3X^2 - Y^2) = X^4 - 6X^2Y^2 + Y^4$	+	–
(4,−4)	$XY(X^2 - Y^2)$	+	–

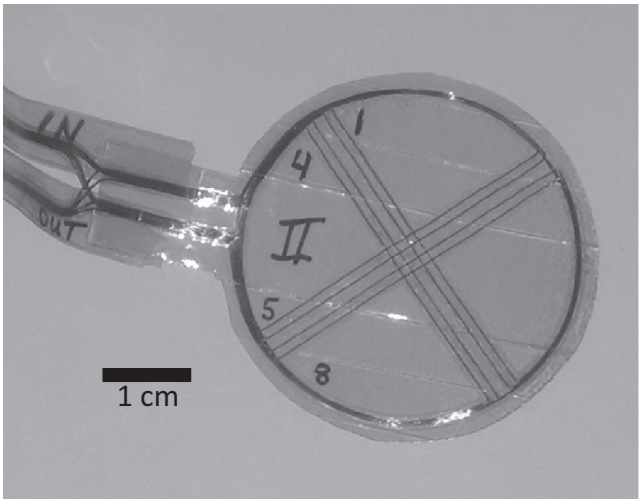

Fig. 3. Photograph of a two-η, two-direction shim plane. Two of these would be used in a 2-direction shim set, one mounted near each pole. This particular shim plane is for Z_0 = 1.9 mm, η = 0.4 and 1.0. Four of these were built for the shim system used in the measurements. The construction method and materials are described in the text.

4. Selectively producing fields

While we have argued that the spherical harmonic fields can be created by the straight wires, more is required for a functional shim set. Each element of the shim set must be separately produced and controlled, so that arbitrary linear combinations of shim fields can be produced to correct any given magnetic field inhomogeneity. To achieve this selective production of shim basis set fields we take advantage of having multiple wires in each of our directions. More than one value of η is available, in addition to symmetry considerations, to select the particular field to be produced.

That this will work for the straight wire functions is apparent from the $C(\eta)$ functions in Table 1, plotted in Fig. 2. For example, if we sought to make (2,1) using wires at locations $\eta = 0.4$ and 1.0 (and symmetry related positions), we would first choose the appropriate current symmetry, which is even in Y and odd in Z. Symmetry considerations alone reduce the possible spurious fields to the T_{4E} term, which would lead to unwanted fourth order harmonic fields. (2,1) is the T_{2E} field, so we consider the plots of C_{2E} and C_{4E} evaluated at $\eta = 0.4$ and $\eta = 1.0$. We have two adjustable parameters at our disposal, the two independent currents, so it should be possible to find a setting of these currents that cancel out the T_{4E} field while producing the desired T_{2E} field, unless our particular choices for wire positions lie at a zero in a relevant C-function. Algebraically, we seek currents $I_{0.4}$ and $I_{1.0}$ such that

$$I_{0.4}C_{2E}(0.4) + I_{1.0}C_{2E}(1.0) <> 0 \text{ and } I_{0.4}C_{4E}(0.4) + I_{1.0}C_{4E}(1.0) = 0. \quad (5)$$

Naturally, it will generally also be possible to find the currents that suppress T_{2E} while producing T_{4E}, and these current settings will allow the creation of the fourth-order fields without making the symmetry-allowed second order fields. More concretely, the function values are $C_{2E}(0.4) = 0.333$, $C_{2E}(1.0) = -0.25$, $C_{4E}(0.4) = -0.225$, and $C_{4E}(1.0) = -0.125$, so that to avoid making (4,1), the current ratio should be $I_{0.4}/I_{1.0} = -0.556$, while to avoid making (2,1) the ratio should be 0.750. The generalization to more wires in each direction is straightforward. More wires will be needed if one seeks to avoid producing symmetry-allowed higher order fields, for example the (6,1) field for the case we were considering above.

5. Construction of straight-wire shim set

In order to characterize the performance of the straight wire shim design, we constructed a two-η, four direction shim set. We chose η values 0.4 and 1.0 on the basis of Fig. 2, in an attempt to optimize our ability to selectively produce the individual fields required to make the traditional harmonic fields. The two η values should be chosen so that they lead to both positive and negative values of the C-functions, which facilitates the cancellations required for the production of individual harmonic fields, as discussed above. The shim set was constructed from four identical two-direction assemblies, one of which is shown in Fig. 3. The wires are 36 gauge (0.13 mm diameter), pressed into the sticky side of 0.025 mm thick Kapton tape. Once the wires in both directions were in position, the wires were covered with a second layer of tape, yielding an assembly about 0.28 mm thick at its thickest points. Two of these were placed near each pole of the magnet, with a 45 degree offset between the members of each pair. The magnet was a 1.6 T dipole magnet, with 5 mm gap. The structure of the magnet limited the outer radius of our shim design to 20 mm. The shims are attached to two 0.125 mm thick copper sheets and mounted on either side of a Delrin structure with a void in the working region of the magnet. The shims are located at an average position of $Z_0 = \pm 1.9$ mm.

With this structure mounted in the magnet, 3 mm of free space remains. The small amount of space in the magnet gap was our motivation to pursue this new space-efficient shim design. Our previous installations using a traditional one-coil-per-term harmonic shim set left only a little over 1.5 mm of working space in the magnet, and these shims only contained the first and second order correction fields. The new shim designs leave much more space, while also providing much higher order corrections.

The currents are controlled by 4 eight channel shim controllers originally used for traditional shim sets containing the eight first and second order terms. These controllers have an output stage built around a power op-amp (OPA025) configured for current feedback using a 0.5 Ω sense resistor in the return (ground) leg of each current channel. In these devices, a voltage setting controls the current value up to a maximum of 2 A per channel. The control voltages were set by computer communication to a microcontroller (PIC32) that in turn controlled eight DAC chips via an SPI bus.

6. Measurement system details

The magnetic fields were measured using a microcoil NMR probe mounted on a computer controlled XYZ stage (Zaber Industries, Canada). The NMR console was based on a single-board NMR system (RadioProcessor, from SpinCore, FL, USA). In-house software handled NMR data acquisition, synchronized with X-Y-Z movements. The NMR probe has a sample coil of 0.35 mm diameter and can accept an NMR sample tube with 0.2 mm ID. The coil and sample are mounted at the end of a slender finger made from 1/32″ (0.8 mm) double-clad circuit board. Doped water is used as the sample fluid to facilitate rapid signal averaging, although in homogeneous fields the single-shot SNR is more than adequate. In this magnet, the NMR frequency is about 67.1 MHz. The actual NMR frequency is used to determine the average field value over the sensitive volume of the small sample.

The magnet is a C-shaped SmCo permanent magnet. Its dimensions are 64 mm × 107 mm × 79 mm and it has 25 mm diameter poles made of vanadium permendur. The weight of the magnet is 4 kg. Mechanical adjustment screws are included to allow the alignment of the pole pieces, which allows the reduction of linear gradients. No thermal insulation or control was employed. The mapping process is fast enough that it avoids significant field drift as the magnet temperature changes. The small drifts in frequency are detected and a straightforward polynomial drift correction is applied to the data.

The field is mapped at 156 points on the surface of a sphere. The size of the NMR probe limits the diameter of this sphere to 1.8 mm. This sphere is 36% of the linear space inside the physical magnet, a relatively large fraction that raises the difficulty of shimming to high homogeneity. As shown in Fig. 4, the map measurement points form 13 circles on the sphere, with 12 points in each circle. The figure only shows the map points in the upper hemisphere and equator. The circle nearest to the $-Z$ pole is mapped first, the one at $+Z$ last. Before each circle of locations is measured, and after the last one, the field is also measured at the center of the sphere. These central points are used to monitor and correct for field drift. The procedure requires about 5 min, depending on the degree of signal averaging. Fig. 4 also shows the location of two wires, at $\eta = 0.4$ and $\eta = 1.0$, and the symmetry-related wires positions, for wires oriented into the page.

7. Results and discussion

Fig. 5 shows the map of the field due to current on the wire parallel to the x-axis at location (Y,Z) = (+0.76 mm,+1.9 mm). This is the $\eta = +0.4$ wire depicted in Fig. 1(a). The data are presented in the order in which they were acquired, so the circle nearest the −Z pole is to the left. A single wire produces a significant amount of linear transverse gradient, which shows up in the map as a sinusoidal variation of 13 cycles, one for each circle. To determine the field due to the current alone, four maps are acquired: a background map with the current off, a map with the current set to +0.5 A, a map taken with the current set to −0.5 A, and a second background map with the current off. The field due to the wire alone is found by subtracting the two current-on maps, which yields the field that would be produced per unit current. (For the data shown in Fig. 5, the current happens to flow in the $-x$ direc-

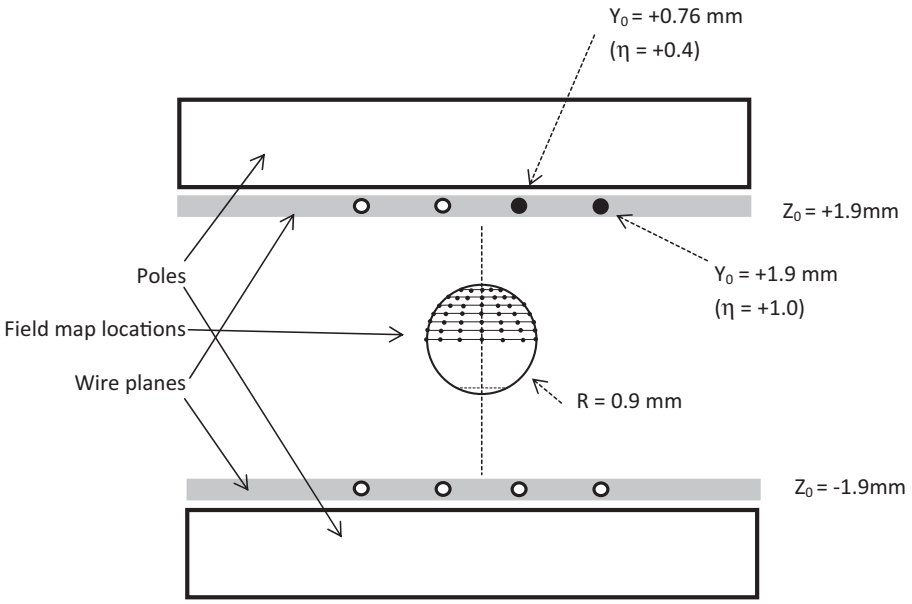

Fig. 4. Geometry of the mapping process. The magnet gap is shown from the side, with poles at top and bottom. Just inside the poles are the planes in which the wires are located. Two wires are shown in cross section in solid black, at locations η = +0.4 and η = +1.0. The locations of the symmetry-related wires are indicated by the open circles on the wire planes. The field map locations in the middle of the gap are indicated by the small points, forming circles on the surface of the sphere of radius 0.9 mm. The map locations are measured starting with the bottom circle first.

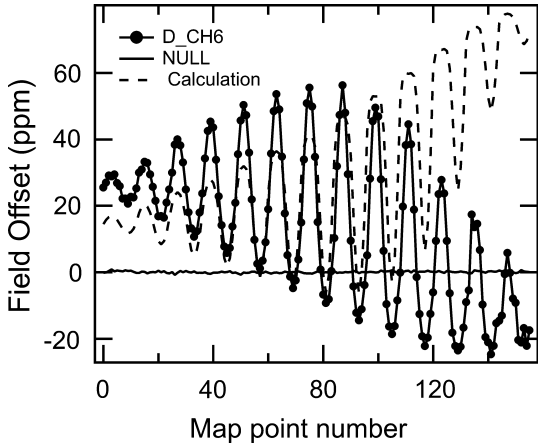

Fig. 5. The field of a single wire. The dots are the measured field values due to the current. The NULL map is the subtraction of two maps made with the current off, one before and one after the current-ON measurements. The dashed line is the field expected from this wire if it were in free space.

tion.) As a check on system stability, the two background maps are subtracted to form a null map, also shown in Fig. 5. The background field maps span about 10 ppm peak-to-peak, and repeated measurements of these maps show a standard deviation of 0.1–0.3 ppm at each point in the map. This should be compared to the one-wire map in Fig. 5, which spans more than 70 ppm.

The dashed line in Fig. 5 shows the field of the wire as calculated using Eq. (2), which is the field expected for a current-carrying wire in free space. The deviation from the measured field is severe, typically many ppm, especially near the poles. The presence of the magnet poles clearly has a profound effect on the fields produced by the currents.

It is possible to make the calculations more closely match the measured fields by allowing the wire locations in the calculation to be significantly shifted toward the center of the magnet. It also is helpful to include image currents, but none of these machinations matches the data at the few ppm level. The discrepancy between the expected and measured fields is most likely due to an effect described four decades ago by Halbach [19]. He was interested in trying to correct the field in a beam-line magnet by having wires placed inside the pole pieces themselves. He found that the fields produced by such wires behaved as if the wires were actually located closer to the center of the magnet and much further from the pole surface. Halbach noted that the poles already were supporting a large field before the adjustment currents were turned on, and when the field due to the currents was added, the pole material responded anisotropically. In the direction of the large background field, the pole material was saturated and did not develop much additional magnetization in that direction, while in the direction perpendicular to the strong field, the pole material could still respond strongly to the field of wire. We can see hints of this effect in our maps and calculations: if we include an image current, offset toward the center of the magnet and much further into the pole than simple geometry would suggest, then the calculated field begins to resemble the measured fields.

Given our facility for measuring field maps, we are happy to take Halbach's suggestion that *calculations* of these effects are likely to fail. Instead, we simply map the individual fields of all 32 wires and then find linear combinations to achieve any desired target field. We find that the built-in Solver in Microsoft EXCEL is adequate to the task. We ask this solver to find the linear combination of one-wire field maps that minimizes the squared deviation from a desired field profile, which could for example be a map calculated using one of the functions in Table 2. The result is a list, or vector, of current values. The resulting vectors of current values show only some evidence of the finely wrought symmetry and algebraic arguments presented earlier. One of the more clear examples is shown in Fig. 6, where the values for currents in the y direction are shown as a function of $\eta = X_0/Z_0$ for the (2,1) and (4,1) shims. The currents on the +Z and −Z sides are shown separately as open and closed symbols, respectively. Broadly speaking, the current values show the expected asymmetry with respect to z and symmetry with respect to x (see Table 2). In addition, the relative signs of the currents at η = 0.4 and 1.0 is in agreement with

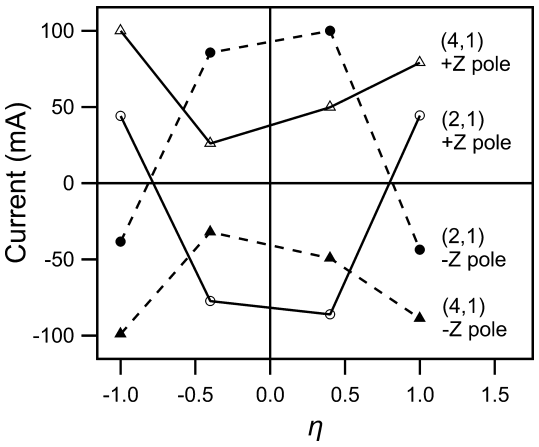

Fig. 6. Current values for the (2,1) and (4,1) shims for wires parallel to the y-axis. These values were determined through the map fitting process described in the text.

the expected ratios $I_{0.4}/I_{1.0} = -0.556$ and +0.750 for (2,1) and (4,1), as discussed previously.

However, the actual ratio values are rather different from the expectations, and the symmetries are not particularly pure. This is probably due to the fitting process compensating for errors in construction and mounting of the physical shim sets. (Other groups of wires, and other shim fields, generally do not exhibit symmetries as clear as those in Fig. 6.) As we will see shortly, the fields that result from this fitting process are very accurate, so we see no advantage in imposing the expected symmetries on the current vectors.

The theoretical discussion of straight-wire fields is useful for understanding that they can form complete shim sets with individual shim control and for guiding construction. However, the detailed functional expressions in Table 1 are not applicable in high-field magnets with pole pieces. This means that we cannot rely on this theory to provide fully correct shim designs, implying that Anderson's approach, as well as a number of other shim design methods, will struggle to provide high-quality high-order fields for such magnets.

The maps of the harmonic fields resulting from our fitting approach are shown in Figs. 7 and 8. The first order maps, in Fig. 7(a), are nearly perfect, with the locations of the points within the sinusoidal pattern themselves forming a regular pattern (i.e., on a common longitude), and the Z field (1,0) showing very flat steps, one for each circle with constant z value. The symbols in the figure are the measured fields, while the lines are calculations of the corresponding functions from Table 2. Each of these fields is the result of a distinct vector of 32 current values. The maximum element of each vector was 200 mA for these data. Panels (b) and (c) show the mapped second order fields. Again, the lines are the calculated Table 2 functions. Here, the maximum shim current value employed was 400 mA. The second order terms are a bit weaker than the first, as expected.

Fig. 8 shows the same kind of map and calculation results for the third and fourth order fields. These were all acquired with a maximum current value of 600 mA. These fields are much weaker. The wires readily make the first-order fields; to make the higher orders, increasingly delicate cancellation of the stronger lower order components must be achieved. The match between map and calculation is visible for the fields shown in Fig. 8. Maps of (3,±3), (4,±3), and (4,4) fields were also acquired, but presentation of that data in the format of Fig. 8 is not helpful in determining if these fields were produced.

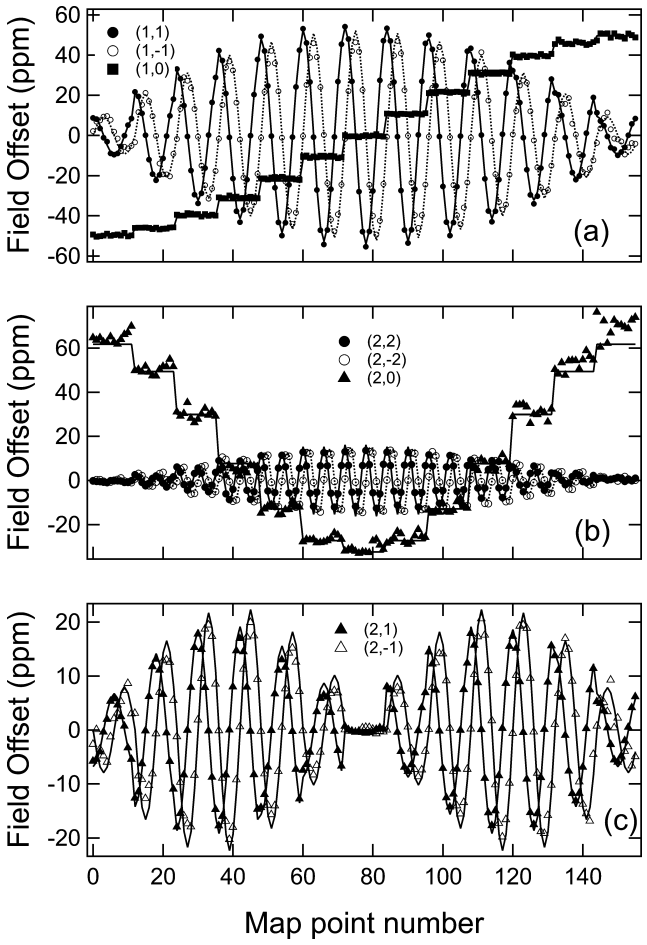

Fig. 7. Maps of the first and second order real-valued spherical harmonic fields created by the straight-wire shims. The symbols are the measured fields due to the currents. The lines show the corresponding functions from Table 2. The agreement is remarkable and indicates a very high purity (and hence orthogonality) in this shim set.

A more quantitative, albeit abstract, assessment of the quality of the mapped harmonic fields is to decompose each map into an expansion based on the real valued spherical harmonic functions, Eq. (4). For the normalization in Eq. (4), the absolute value of the expansion coefficient values are indicative of the peak-to-peak variation in the map that can be attributed to each term. The purity of the first order fields is clearly shown by their harmonic coefficients. For example, for the (1,0) field, the largest coefficient is (1,0) = 71.0 ppm, while the next largest "impurity" coefficient is (3,0) = 1.87 ppm, only 2.6% of the expected field. Table 3 gives this same coefficient data for all 23 harmonic fields in our shim set. The (1,1) and (1,−1) fields are even more pure than the (1,0), with maximum impurity contributions of 0.5% and 1.2%, respectively. The second order fields are only a little worse, with maximal impurity contents of 2.5–8%. The trend continues for the third and fourth order shim fields, with the impurities getting quite large. Note, however, that only two shims, (4,−1) and (4,4) show impurity contents above 55%. For some third and nearly all fourth order shims in Table 3, the expected harmonic coefficient is not much larger than our mapping reproducibility, and the "large" impurities have significant contributions from measurement noise. To the extent that the impurities are really present, they can be compensated for during the shim adjustment process.

Tables of all harmonic impurity contents are provided in the supplementary materials.

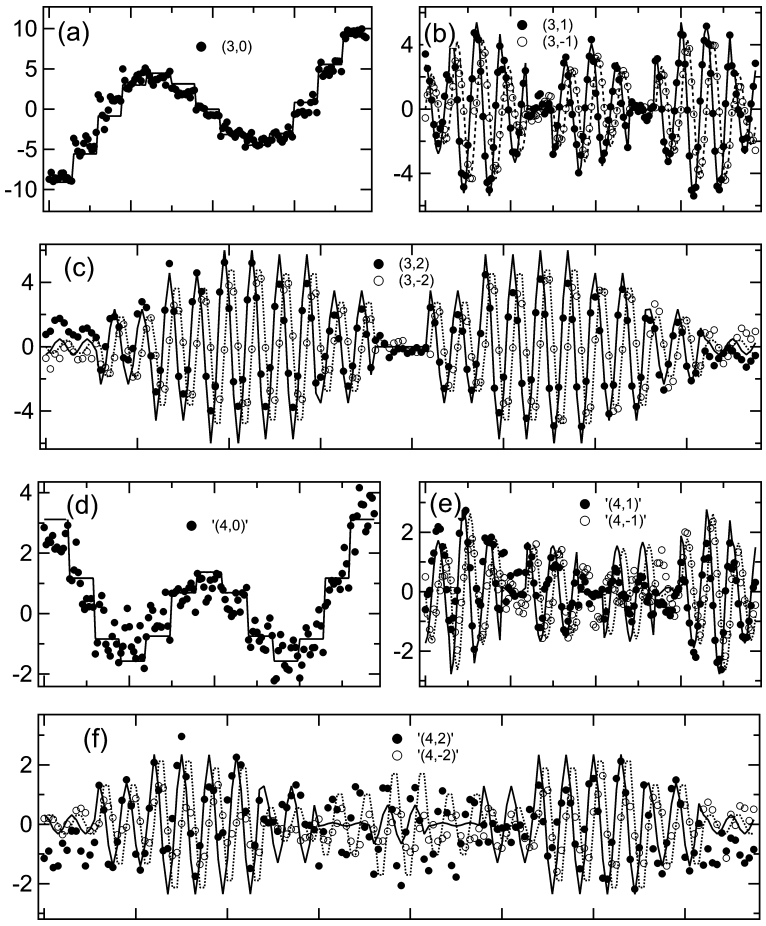

Fig. 8. Maps of the third and fourth order real-valued spherical harmonic terms. This figure was created in the same way as Fig. 7.

Table 3
Largest impurities in each shim. Scale corresponds to the harmonic fields in Figs. 7 and 8.

Shim	Coefficient	Impurity	Coefficient	(%)
(1,0)	71.0	(3,0)	1.87	2.6%
(1,1)	113.4	(3,1)	0.53	0.5%
(1,−1)	99.2	(3,−1)	1.14	1.2%
(2,0)	73.8	(2,2)	−4.06	5.5%
(2,1)	32.5	(1,1)	0.81	2.5%
(2,−1)	36.6	(4,−1)	0.97	2.7%
(2,2)	24.6	(4,2)	1.48	6.0%
(2,−2)	29.9	(4,−2)	2.32	7.8%
(3,0)	8.62	(3,2)	−1.37	15.9%
(3,1)	8.28	(3,3)	−0.59	7.1%
(3,−1)	6.31	(2,−1)	0.68	10.8%
(3,2)	8.13	(1,0)	−0.84	10.3%
(3,−2)	7.71	(3,1)	0.48	6.2%
(3,3)	1.31	(1,0)	−0.28	21%
(3,−3)	−1.08	(3,−1)	0.46	43%
(4,0)	2.48	(4,2)	−0.90	36%
(4,1)	2.64	(1,0)	−0.83	31%
(4,−1)	1.92	(1,−1)	1.84	96%
(4,2)	3.07	(4,0)	−0.70	23%
(4,−2)	1.69	(1,−1)	0.41	24%
(4,3)	1.06	(4,2)	−0.58	55%
(4,−3)	0.97	(4,2)	0.53	55%
(4,4)	0.57	(4,2)	−0.67	117%

The harmonic content of the shim fields is of practical importance because it measures the breakdown of orthogonality in the shim set. The harmonic coefficients can be used to improve the orthogonality by adjusting the current value vectors for each shim. However, it is good to keep in mind that orthogonality is defined for a fixed choice domain, in this case, the 156 points on the surface of a 1.8 mm diameter sphere centered in the magnet gap.

Another consideration of importance in shim design is coil efficiency, the strength of the shim fields per unit current. Inefficient shims require large currents which may lead to heating and field drift. As a practical matter, shimming our magnet did not lead to unmanageable heating, as shown below, so we have not optimized our design for efficiency. Larger magnets, in which the shim fields will be weaker, may require more attention to efficiency. For the multi-wire shims, a convenient figure of merit is the sum of the squares of the 32 currents. For the X, Y and Z fields shown in Fig. 7, the sums are 0.30 A^2, 0.39 A^2, and 0.50 A^2. The second order fields required sums in the range 0.75–1.73 A^2, the third and fourth order fields 1.30–2.84 A^2. The resistance of a typical wire is very low, less than 0.5 Ω.

Our two-η, four direction shim set has 32 independent currents and can produce all 1st through 4th order spherical harmonic fields, excluding (4,−4), a total of 23 harmonic fields. Hence, there appear to be 9 unused degrees of freedom, and one may ask if additional fields could be produced. The answer is No. Looking at Table 1, it is clear that any one of the four wires directions could be used to produce the Z field, so there are three redundancies that account for three of the extra degrees of freedom. Similarly, there is redundancy in the X and Y fields, which could just as well have been produced by the wires orientated along the diagonals. The four wire directions are capable of producing 8 first order fields, but only three of these can be linearly independent. For the second order fields, we showed that two wire directions were enough to

create all but the (2,−2) field. If we had started from the diagonal wires, we could have produced all but the (2,2) field. This accounts for three degenerate degrees of freedom at order two. There is one more degenerate degree of freedom at order three, and none at order four. Although it would seem that a 32 wire shim set should be able to make up to 32 harmonic fields, we must accept a certain level of redundancy that lowers this number. The redundancy can be utilized to reduce the currents required by spreading them out over the appropriate other wires.

A further item of interest may be the applicability of straight-wire approach in the popular Halbach configuration, cylindrical bore magnets with a transverse field, typically without poles. The cylindrical environment does not readily admit straight wires in multiple orientations. It is not clear that helical wires will have symmetries that map well only the real-valued spherical harmonic functions which would indicate that such wires could produce complete shim sets. Active shim sets for Halbach magnets tend to consist of circular patterns arranged on a cylindrical surface. We do not yet have a new design for use in Halbach magnets.

Taken together, Figs. 7 and 8 and Table 3 show that very high quality correction fields, extending to high order, can be made by our new space-efficient shim design. In principle, we could use the straight-wire fields themselves (the functions in Table 1, extended to all four directions) to correct our magnet. In fact, this is what we do to achieve our first pass correction, which is done in the magnet with the probe and sample removed. When the probe and sample are in place however, we can switch to using our spherical harmonic fields for shimming and utilize their orthogonality and the existing knowledge base covering the art of shimming for high-resolution NMR.

8. Application to high resolution NMR in a compact permanent magnet

To demonstrate that the shims can actually be used in the lab, we have constructed a rudimentary probe for our magnet. This probe has a Delrin body that fits snugly into the 3 mm open space between the copper sheets that hold the shims. The probe contains a coil of 4 turns of 36 gauge common magnet wire, wound on the outer surface of a 1.8 mm OD, 1.5 mm ID tube (Vitrocom). Samples are sealed into smaller tubes, 1.2 mm OD and 1.0 mm ID (Vitrocom), which are inserted into the larger tube and held in place by two layers of thin Kapton tape wrapped on the OD of the sample tube. There is clearly room for improvements to this design, particularly as the susceptibility of the RF coil is uncompensated.

Field drift is a much larger problem for high-resolution NMR than it is for field mapping and shim development. To suppress this drift, the magnet was enclosed in rigid foam insulation (0.88 m^2 K/W, or R5 in the US). The shim currents caused some warming but the bigger effect was changes to the room temperature. To combat these effects, the shims were left on and the room cooling system was turned off. This resulted in a long interval of magnet stability each day. Aluminum foil was used to provide some degree of RF shielding. There was no magnetic shield employed.

The individual harmonic field strengths could be adjusted manually via a computer interface. The software took the user-requested spherical harmonic shim setting values and converted these to the required 32 current values. We found that the shims could be adjusted one by one, for the most part, with little interaction. This is probably the result of our efforts toward optimizing the orthogonality of the shim set, although it should be noted that our sample volume is not entirely the same as the mapping volume used for orthogonalization. We do not yet have any automatic shimming algorithms implemented for this new system. It is probable that our results are limited by our skill and patience in finding the optimal shim settings.

Despite the rough construction of our probe and nascent shim adjustment methodology, we were still able obtain remarkable improvements in the linewidth for our samples, as shown in Fig. 9. For panels (a) and (b) the sample is acetonitrile and the spectra are single shot acquisitions. The unshimmed line in panel (a) has a FWHM of 670 Hz (10 ppm). Our best shimming result is shown in panel (b), where the FWHM is 1.5 Hz (<25 ppb), a more than 400-fold improvement. The peak is wider than desired at the baseline (15 Hz at 10% height), but this extra width has the appearance of a slightly wider line with an otherwise well-behaved baseline. We can speculate that the wide component of the peak is the result of not having found the optimum setting for our higher order shim fields. It may also be the case that our somewhat naïve probe construction is introducing error terms that are not included in our shim set. The importance of Fig. 9 is that it shows that the new shim design can provide relevant levels of homogeneity improvement without causing undue heating. This is a necessary condition for the new shim design to be viable.

Anticipating possible applications, in which minority fluid components are often of interest, Fig. 9(c) shows the spectrum of an old red wine sample. The shim settings were adjusted a small amount for this sample, as is usual for high-resolution NMR. The small, poorly phased peaks offset by ~1 ppm to either side of the large peak are 60 Hz sidebands, which may arise from our shim current supplies, pickup of stray fields by the unfiltered shim lead wires, or from the magnetic environment in the lab. (Panel (b) also shows small sidebands.) In the red wine spectrum, the methyl peak (~1 ppm) of the alcohol is clearly separated from the main water peak, at 4.8 ppm, indicating that we do have manageable baseline spreading, but the methyl triplet is far from resolved. The areas of the methyl signal and water lines can be compared. Their ratio is 0.074, somewhat lower than the roughly 10% value expected for 13.5 vol% wine. Our wine sample is somewhat aged and of murky provenance.

Fig. 9 shows that the new shim design can move from proof of principle to a more applied lab setting. The results are certainly promising enough to warrant further work, including improved

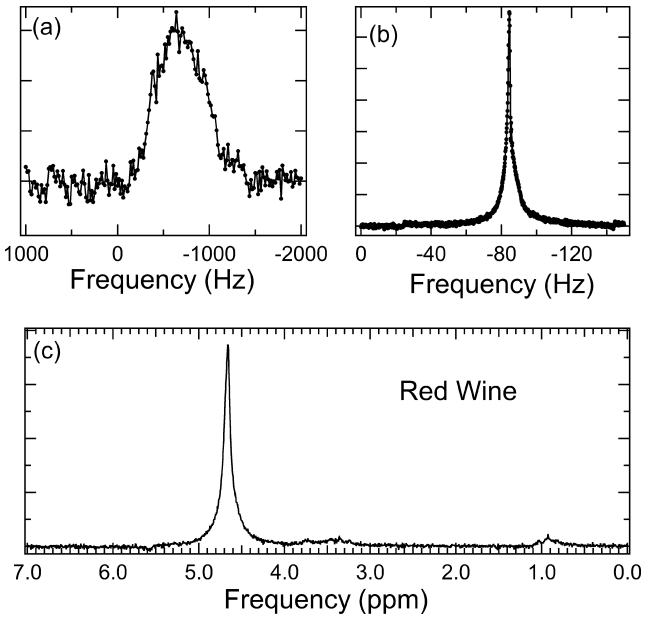

Fig. 9. Spectra from 1.0 mm diameter samples. For panels (a) and (b) the sample fluid is acetonitrile and the data are a single acquisition. In panel (a) the spectrum with the shim currents turned off is shown; the line has a FWHM of 670 Hz. In panel (b), the spectrum with the shims adjusted is shown. The FWHM is 1.5 Hz, while the width at 10% height is 15 Hz. Panel (c) shows the spectrum of a sample of red wine. The ^{1}H frequency in this magnet is 67.1 = MHz.

probe design and construction and more sophisticated shim optimization protocols. It should be kept in mind that the results in Fig. 9 come after a short period of time working with a completely new form of shim set, and we are not utilizing slow sample spinning to improve the spectral resolution. We anticipate substantial further improvements in spectral performance using our new approach to shim design.

9. Summary and conclusion

In this article, the general principles of the work of Anderson more than 50 years ago were identified and extended into a more expansive framework which supports the design of highly space-efficient shims capable of high order corrections. The new design concept is of groups of straight wires traversing the space-limited region across the gap of a dipole magnet, avoiding the wire crossings required by traditional designs. Each wire carries its own independently controlled current. A theoretical discussion was presented that links the fields of straight wires to the real-valued spherical harmonic fields familiar to NMR shim practitioners.

Measurements of the fields of individual wires were shown to differ significantly from the expected form, an effect attributed to the anisotropic response of pole materials driven well into saturation. Despite undermining the ability to calculate the currents required to achieve any particular field, the complicated pole material response does not undermine the basic symmetry and completeness arguments that indicated the new approach should work as a complete shim set. The fields of all the wires were mapped, and combinations of these maps were found numerically so that the traditional spherical harmonic fields could be produced. Measurements of the resulting fields found them to be of high purity and of substantial strength.

The shim set was used in an early prototype NMR spectroscopy system with a 1 mm sample size in a 5 mm gap magnet. The new shims were adjusted manually to achieve FWHM line width of 1.5 Hz (<25 ppb). A single shot spectrum of a red wine sample showed useful resolution, although more work will be required before legitimately high-resolution NMR can be claimed. These first results clearly show that the new shim design is practical and warrants a more sophisticated prototype system in which to show its full power.

Acknowledgments

AFM thanks Fred McDowell for help with data acquisition. MSC thanks Washington University for sabbatical leave support.

Appendix A. Supplementary material

Supplementary data associated with this article can be found, in the online version, at http://dx.doi.org/10.1016/j.jmr.2017.04.013.

References

[1] M.J.E. Golay, Field homogenizing coils for nuclear spin resonance instrumentation, Rev. Sci. Inst. 29 (1958) 313–315.
[2] W. Anderson, Electrical current shims for correcting magnetic fields, Rev. Sci. Inst. 32 (1961) 241–250.
[3] R. Turner, A target field approach to optimal coil design, J. Phys. D Appl. Phys. 8 (1986) L147–L151.
[4] M. Engelsberg, R.E. De Souza, C.M. Dias Pazos, The limitations of a target field approach to coil design, J. Phys. D Appl. Phys. 21 (1988) 1062–1066.
[5] F. Qi, X. Tang, Z. Jin, L. Wang, D. Zu, W. Wang, A new target field method for optimizing longitudinal gradient coils' property, PIERS Online 3 (2007) 865–869.
[6] W. Liu, X. Tang, D. Zu, A novel target-field approach to design bi-planar shim coils for permanent-magnet MRI, Concepts Magn. Reson B 37B (2010) 29–38.
[7] S. Crozier, D.M. Doddrell, Gradient coil design by simulated annealing, J. Magn. Reson. A103 (1993) 354–357.
[8] J. Chladek, P. Konzbul, P. Osmera, A. Gottvald, Evolutionary and genetic optimization of NMR gradient and shim coils, IEEE Trans. Magn. 36 (2000) 1102–1105.
[9] Y. Terada, D. Tamada, K. Kose, Development of a temperature-variable magnetic resonance imaging system using a 1.0 Tesla yokeless permanent magnet, J. Magn. Reson. 212 (2011) 355–361.
[10] M. Poole, R. Botwell, Novel gradient coils designed using a boundary element method, Concepts Magn. Reson. 31B (2007) 162–175.
[11] S.E. Ungersma, H. Xu, B.A. Chronik, G.C. Scott, A. Macovski, S.M. Conolly, Shim design using a linear programming algorithm, Magn. Res. Med. 52 (2004) 619–627.
[12] F. Tang, F. Liu, F. Freschi, Y. Li, M. Repetto, L. Giaccone, Y. Wang, S. Crozier, An improved asymmetric gradient coil design for high-resolution MRI head imaging, Phys. Med. Bio. 61 (2016) 8875.
[13] P.T. White, J.G. Korvink, H.J. Shah, M.S. Poole, Theoretical design of gradient coils with minimum power dissipation: accounting for the discretization of current density into coil windings, J. Magn. Reson. 235 (2013) 85–94.
[14] D. Tamada, T. Nakamura, K. Kose, A gradient coil design for a high-temperature superconducting bulk magnet using the finite difference method, Supercond. Sci. Tech. 28 (2015) 095010.
[15] A.F. McDowell, E. Fukushima, Ultracompact NMR: H1 spectroscopy in a sub-kilogram magnet, Adv. Magn. Res. 35 (2008) 185–195.
[16] E. Danieli, J. Perlo, B. Bluemich, F. Casanova, Small magnets for portable NMR spectrometers, Angew. Chem. Int. Ed. 49 (2010) 1–4.
[17] A.F. McDowell, Magnetic Field Correction System, US Patent 9285441, 2016.
[18] G. Arfken, Mathematical Methods for Physicists, Wiley, New York, 1985, p. 666.
[19] K. Halbach, Field correction windings for iron magnets, Nucl. Inst. Meth. 107 (1973) 515–528.